chemistry

MDPI

Article

The Antimicrobial and Mosquitocidal Activity of Green Magnesium Oxide Nanoparticles Synthesized by an Aqueous Peel Extract of *Punica granatum*

Amr Fouda [1,*], Khalid S. Alshallash [2,*], Mohammed I. Alghonaim [3], Ahmed M. Eid [1], Ahmed M. Alemam [1], Mohamed A. Awad [4] and Mohammed F. Hamza [5,6]

[1] Botany and Microbiology Department, Faculty of Science, Al-Azhar University, Nasr City, Cairo 11884, Egypt
[2] College of Science and Humanities—Huraymila, Imam Mohammed Ibn Saud Islamic University (IMSIU), Riyadh 11432, Saudi Arabia
[3] Department of Biology, College of Science, Imam Mohammad Ibn Saud Islamic University (IMSIU), Riyadh 11623, Saudi Arabia
[4] Department of Zoology and Entomology, Faculty of Science, Al-Azhar University, Nasr City, Cairo 11884, Egypt
[5] School of Nuclear Science and Technology, University of South China, Hengyang 421001, China
[6] Nuclear Materials Authority, El-Maadi, Cairo 530, Egypt
* Correspondence: amr_fh83@azhar.edu.eg (A.F.); ksalshallash@imamu.edu.sa (K.S.A.)

Abstract: An aqueous extract of *Punica granatum* peel was used as a biocatalyst for magnesium oxide nanoparticle (MgO-NP) synthesis, which was characterized via UV-Vis spectroscopy, TEM, EDX, FT-IR, XRD, DLS, and zeta potential. Data showed the efficacy of the plant aqueous extract in forming spherical, crystalline-nature, well-arranged MgO-NPs with sizes in the range of 10–45 nm with average sizes of 24.82 ± 8.85 nm. Moreover, EDX analysis revealed that the highest weight and atomic percentages were recorded for Mg and O ions. The green synthesized MgO-NPs showed antimicrobial activity against *Bacillus subtilis*, *Staphylococcus aureus*, *E. coli*, *Pseudomonas aeruginosa*, and *Candida albicans* in a concentration-dependent manner with clear zones in the range of 8.7 ± 0.6 to 19.7 ± 0.5 mm with various concentrations. Also, the MIC value was varied to be 25 µg mL^{-1} for Gram-negative bacteria, *B. subtilis*, and *C. albicans* and 50 µg mL^{-1} for *S. aureus*. Moreover, MgO-NPs showed high activity against the 3rd-instar larvae of *Culex quinquefasciatus*. The mortality percentages were concentration- and time-dependent. Data analysis showed that the highest mortality was 88.3 ± 3.2%, attained at a concentration of 100 µg mL^{-1} after 72 h. Also, all originated pupae were malformed and did not hatch to adults, with mortality percentages of 100% at all concentrations. Overall, the *P. granatum*-mediated MgO-NPs showed promising activity in inhibiting the growth of pathogenic microbes and the hatching of *C. quinquefasciatus* larvae to adults.

Keywords: plant-based nanoparticles; magnesium oxide; characterization; antimicrobial; larvicidal

Citation: Fouda, A.; Alshallash, K.S.; Alghonaim, M.I.; Eid, A.M.; Alemam, A.M.; Awad, M.A.; Hamza, M.F. The Antimicrobial and Mosquitocidal Activity of Green Magnesium Oxide Nanoparticles Synthesized by an Aqueous Peel Extract of *Punica granatum*. *Chemistry* **2023**, *5*, 2009–2024. https://doi.org/10.3390/chemistry5030136

Academic Editor: Simona Concilio

Received: 25 July 2023
Revised: 28 August 2023
Accepted: 6 September 2023
Published: 12 September 2023

1. Introduction

The spread of epidemics transmitted by drug-resistant pathogens exacerbates global mortality and morbidity rates, especially with antibiotic-resistant bacteria, as well as insects that transmit viruses and bacteria that threaten humans with serious diseases (vector-borne illnesses) such as epidemic typhus, dengue fever, and epidemic encephalitis [1]. The severity of these threats increased after the rise in vector resistance to drugs, so it became necessary to devise innovative methods or develop drugs to combat insect-borne diseases and antibiotic-resistant microbes. Nanotechnology presents a strong candidate for developing new nano-based drugs that can potentially treat these infections [2,3]. Studies show that more than 70% of pathogenic bacterial strains have acquired resistance to at least one major category of prescribed antibiotics while only a small percentage of these pathogens have become resistant to all antibiotics [4]. The global increase in the prevalence

of life-minatory severe diseases due to the spread of multi-drug-resistant pathogens requires us to develop these drugs and invest in the search for innovative treatments, especially bio-derived nanoparticles (NPs), to eliminate these resistant microbes [5]. On the other hand, millions of people die annually due to mosquito-borne diseases such as malaria (caused by the mosquito-borne *Plasmodium parasite*), which affects more than 220 million cases annually worldwide. In 2018, 405,000 people died from malaria [6]. One of the most dangerous mosquitoes is *Culex quinquefasciatus*, often found in countries with warm climates and tropical and subtropical regions globally. It can adapt to the urban environment, and it is found in human dwellings. It is one of the most abundant types of peridomestic mosquitoes globally. This mosquito is considered the main vector of serious diseases such as the West Nile virus, second-flavivirus St. Louis encephalitis, and phlebovirus Rift Valley fever virus alongside avian malarial parasites and filarial worms [7,8].

Nanomaterials have been of interest recently, especially NPs with chemical and physical properties that distinguish them from the parent materials, and these exceptional properties have imposed their application in many fields such as the food industry, agriculture, electronics, catalysis, medicine, and pharmaceuticals [5,9]. Recently, green nanotechnology has emerged as an alternative to energy-consuming chemical and physical manufacturing methods that contain potentially toxic materials and are costly. Biological methods are environmentally safe, as microorganisms or plants are used to synthesize NPs with an average size of up to 100 nanometers, and they have a fundamental role in bioengineering and nuclear energy [10]. Plants and microorganisms have huge potential for bioreduction and the production of stable NPs thanks to coating agents, with the possibility of the extra/intracellular synthesis of NPs [11]. In addition, plant synthesis methods are the best biological options for producing NPs at a low cost, easily, and in large quantities, with better control over their size, shape, and biocompatibility, which allows them to be applied medically in the treatment of cancer, drug delivery, and as antibacterial and antifungal agents, as well as enabling their successful use in insecticide [12].

Phyto-based magnesium oxide nanoparticles (MgO-NPs), in addition to biocompatibility and biodegradation, have shown many distinctive chemical and physical properties, such as high stability, redox attributes, and cationic ability [13]. They have been considered potential therapeutic alternatives to be used medically to eliminate microbial biofilms and combat microbes and antibiotic resistance, in addition to recognizing their anti-cancer properties, repellence, and larvicidal activities [14,15]. The preparation of MgO-NPs from different plant species has been recently reported, e.g., *Arachis hypogaea* L., *Rosmarinus officinalis* L., *Trigonella foenum-graceum*, and *Manihot esculenta* [16]. Therefore, when considering the biological production of metal/metal oxide NPs, plant biodiversity is taken into account, as plant extracts may contain substances capable of reducing mineral salts and leading to the formation of NPs, and the further investigation of the properties of these nanostructures for use in diagnosis and therapy is underway [17]. Recently, biogenic MgO-NPs manifested premium antibacterial properties against Gram-negative bacteria (*Escherichia coli* and *Klebsiella pneumoniae*) and Gram-positive bacteria (*Staphylococcus aureus* and *Enterococcus faecalis*), in addition to showing their considerable larvicidal potential against larvae of *Aedes albopictus* and *Aedes aegypti* [18].

Punica granatum L. "pomegranate" is a member of the Punicaceae family and has been used in folk medicine to treat many ailments such as fever, bleeding, diarrhea, dysentery, and male infertility. Pomegranate contains phenolics (punicalagin, punicic acid, ellagitannins, and ellagic acid) in different parts such as the arils, seeds, leaves, peel, roots, and flowers, and these phenols give pomegranate its health-promoting benefits against diseases such as cancer, Alzheimer's, obesity, arthritis, diabetes, and cardiovascular and cardiovascular diseases [19].

Pomegranate peel contains a wide range of biologically active substances, such as punicalin, punicalagin, ellagitannins, and polyphenols, that have been employed in forming diverse medicinal, cosmetic, and food compounds and have also shown antimicrobial and antioxidant characteristics and been used for the synthesis of NPs [20].

Considering plant nanotechnology, the present study aimed to biosynthesize MgO-NPs using pomegranate peel extract and characterize these NPs via UV-Vis spectroscopy, transmission electron microscopy (TEM), Fourier-transformed infrared (FTIR), energy-dispersive X-ray (EDX), dynamic light scattering (DLS), X-ray diffraction (XRD), and zeta potential. The phyto-derived MgO-NPs were investigated for their antimicrobial potential against selected pathogens including Gram-positive bacteria, Gram-negative bacteria, and unicellular fungi. Moreover, the larvicidal efficiency of plant-based MgO-NPs was assessed against *Culex quinquefasciatus* mosquitoes. In this work, the novelty lies in the successful synthesis of MgO-NPs utilizing plant waste (*P. granatum*-peel aqueous extract) as a green and eco-friendly method. This approach not only showcases a sustainable and cost-effective means of NP production but also introduces MgO-NPs with exceptional antimicrobial properties. These NPs exhibited high activity against various pathogenic microorganisms at low concentrations, which was a remarkable achievement. Furthermore, the significant larvicidal activity resulting in high mortality rates and the prevention of adult emergence in *C. quinquefasciatus* larvae demonstrates a unique and promising aspect of this research. This combination of green synthesis, potent antimicrobial action, and larvicidal effects makes this work truly innovative.

2. Materials and Methods

2.1. Material Used

Magnesium nitrate hexahydrate ($Mg(NO_3)_2 \cdot 6H_2O$), which is used as a precursor for MgO-NP synthesis, NaOH, and media components, was analytical-grade and purchased from Sigma-Aldrich, Cairo, Egypt. All reactions in the current study were achieved by using distilled water (dH_2O).

2.2. Biosynthesis of MgO-NPs Using Punica Granatum

2.2.1. Aqueous Extract Preparation

To prepare the reducing agent for forming MgO-NPs, the peels of *P. granatum* were collected and washed thrice with dH_2O to remove any adhering debris. The peels were then dried at 40 °C and ground to form a powder. Next, 5 g of the prepared powder was mixed with 100 mL of dH_2O and heated for 60 min at 55 °C using a magnetic stirrer (rpm = 120). After heating, the mixture was filtered and then centrifuged at 6000 rpm for 10 min. The supernatant was collected and used as a reducing, capping, and stabilizing agent to synthesize MgO-NPs.

2.2.2. Plant-Mediated MgO-NPs Synthesis

In this method, an aqueous peel extract of *P. granatum* (10 mL) was mixed with dH_2O (90 mL) containing 51.3 mg of $Mg(NO_3)_2 \cdot 6H_2O$ to obtain a final concentration of 2 mM. The mixture was stirred for one hour at 40 °C, with the pH of the mixture being 8, using 1 N NaOH. After being left overnight, the brown precipitate, which represented $Mg(OH)_2$, was collected and rinsed with dH_2O to remove any impurities before being calcinated at 200 °C for four hours to form MgO-NPs [16]. The plant extract without metal precursor, as well as the dH_2O containing $Mg(NO_3)_2 \cdot 6H_2O$, was running with the experiment as a control.

2.3. Characterizations

UV-Vis spectroscopy (JENWAY-6305, Staffordshire, UK) was used to monitor the color change from pale-red to brown. In this method, 2 mL of the formed solution was put in a cuvette, and we measured its absorbance at varied wavelengths in the range of 200–600 nm to detect the maximum surface plasmon resonance (SPR). A Cary 630 Fourier-transform infrared (FT-IR) spectrometer (Tokyo, Japan) was used to determine the functional groups in plant aqueous extract and phytosynthesized MgO-NPs. Here, 300 mg of synthesized MgO-NPs was mixed with KBr and pressed into a disc, after which it was examined at wavenumbers of 400 and 4000 cm^{-1}. Additionally, a KBr disc was loaded with a few drops of plant aqueous extract and scanned at the same wavenumber. The crystallinity nature

of synthesized MgO-NPs was detected using X-ray diffraction (XRD, X' Pert Pro, Philips, Eindhoven, the Netherlands) in the range of two theta values: 10^0–80^0. The operation conditions were as follows: Cu-Kα was the source of the X-ray, λ (X-ray wavelength) was equal to 1.54 Å, and current and voltage were adjusted at 30 mA and 40 Kv, respectively.

The average crystallite size of plant-synthesized MgO-NPs was detected using the Debye–Scherrer equation [21]:

$$\text{Average crystallite size} = \frac{0.9 \times 1.54}{\beta \cos\theta} \quad (1)$$

where 0.9 is the Debye–Scherrer constant, 1.54 is the X-ray wavelength (λ), β is half of the maximum intensity, and θ is the Bragg's angle.

The shape and size of the plant-synthesized MgO-NPs were examined using transmission electron microscopy (TEM, JEOL 1010, JEOL, Tokyo, Japan). After we deposited a few drops containing MgO-NPs with colloidal dispersion onto the TEM grid (carbon–copper), the loaded grid was subjected to vacuum desiccation overnight followed by being transferred to the TEM holder for sample analysis. In addition, the elemental composition of synthesized MgO-NPs was detected by using energy-dispersive X-ray technology (EDX, JEOL, JSM-6360LA, Thermo-Fisher Scientific, Tokyo, Japan). In a vacuum, a sputter coater was used to apply a gold coating onto an EDX holder after being loaded with a small amount of NP dispersion.

Finally, the size, size distribution, and polydispersity index (PDI) of MgO-NPs were quantified by using dynamic light scattering (DLS). In this analysis, the MgO-NPs were dissolved in high-purity H_2O (Milli-Q H_2O) to prevent the release of additional peaks or shadows during scattering. The charge of the NPs' surfaces was further checked using a zeta-sizer (Nano-ZS, Malvern, UK) after it had been distributed in Milli-Q H_2O.

2.4. Antibacterial Activity

Using the agar well diffusion method, the activity of green synthesized MgO-NPs in inhibiting the growth of pathogenic bacteria was evaluated [22]. The pathogenic bacterial strains used were represented by Gram-positive bacteria (*Bacillus subtilis* ATCC6633 and *Staphylococcus aureus* ATCC6538), Gram-negative bacteria (*Pseudomonas aeruginosa* ATCC9022 and *Escherichia coli* ATCC8739), and unicellular fungi (*Candida albicans* ATCC 10231). In this method, each bacterial strain was refreshed on nutrient agar media (containing (in g L^{-1} quantities) the following: peptone, 5; beef extract, 3, NaCl, 5, and agar, 15) for 24 h at 37 °C whereas *C. albicans* was refreshed on Sabouraud dextrose agar (containing (in g L^{-1} quantities) the following: dextrose, 40; peptone, 10; and agar, 15; and 1 L dH_2O) and incubated at 35 °C for 24 h. After that, a single colony was picked up via sterilized swap and reinoculated uniformly over the Muller–Hinton agar plate before we made five wells (6 mm) in each plate. Different concentrations (200, 100, 50, 25, and 12.5 μg mL^{-1}) of plant-synthesized MgO-NPs were performed to check their activity. Approximately 100 μL from each concentration was put in a well, and we kept each plate in the refrigerator for one hour before it was incubated at 37 °C for 24 h. The results were recorded in terms of the diameter of clear zones formed around each well (in mm). The lowest concentration that formed a clear zone was recorded as the minimum inhibitory concentration (MIC) [23]. The experiment was achieved in triplicate.

2.5. Mosquitocidal Activity

The larvae of *Culex quinquefasciatus* (family: Culicidae) were obtained from the Medical Entomology Lab, Dokki, Giza, Egypt and were then further reared in the Animal House at the Department of Zoology and Entomology, Faculty of Science, Al-Azhar University, Cairo, Egypt according to Kauffman et al. [24]. The laboratory conditions for rearing larvae to procure adults were as follows: the temperature was 27 ± 2 °C, relative humidity was 75–85%, and photoperiod conditions were 14: 10 light: dark. The activity of plant-

synthesized MgO-NPs was assessed using 3rd-instar larvae and checked until these larvae formed pupae and hatched into adults.

In this experiment, 25 *C. quinquefasciatus* of 3rd-instar larvae were put into a glass beaker containing 250 mL of dechlorinated H_2O for 24 h and mixed with different concentrations (100, 75, 50, 25, and 10 µg mL^{-1}) of synthesized MgO-NPs. The experiment was replicated five times for each NP concentration against 3rd-instar larvae. A glass cup containing dechlorinated H_2O without MgO-NPs served as a control. Each mortality percentages was calculated from the average of five replicas after different contact times (24, 48, and 72 h) by using the following equation [25]:

$$\text{Mortality } \% = \frac{\text{Number of larvae dead}}{\text{Number of larvae treated}} \times 100 \quad (2)$$

The mortality percentages of pupae and adults were calculated based on the converted larvae after 72 h of treatment.

2.6. Statistical Analysis

The data obtained in this study are presented as the average values from three separate replicates, and were subjected to statistical analysis utilizing the SPSS v17 software package. The mean differences among the treatments were assessed using either *t*-tests or analyses of variance (ANOVAs) followed by the Tukey HSD test at a significance level of $p < 0.05$.

3. Results and Discussion

3.1. Characterizations

3.1.1. UV-Vis Spectroscopy

The synthesis of MgO-NPs using an aqueous extract of *P. granatum* (pomegranate) peel appears to have been effective, according to the data. For magnesium ions to have been reduced and stabilized into nanoscale oxide particles (MgO-NPs) shows that the peel extract includes chemicals that can facilitate this process. Pomegranate peels are a rich source of flavonoids, phenolics, alkaloids, tannins, saponins, terpenoids, and steroids, which play an important role in the biofabrication of NPs [26]. Before the biosynthesis of MgO-NPs, different parameters including plant extract concentrations, pH values, and metal precursor concentrations were primarily investigated to select the optimum conditions for the biosynthesis of MgO-NPs based on the intensity of color changes. Data showed that the optimum plant extract ratio that gave the maximum color change was 1:9 (1 mL plant extract: 9 mL dH_2O containing metal precursor), with an alkaline pH value (8) and metal precursor concentration of 2 mM. Recently, the optimum pH value for the green synthesis of MgO-NPs was optimized at 8 [27]. Variations in pH values can modify the charges of biomolecules found in plant extracts, consequently impacting their reducing capacity [13].

Under these optimum conditions, the presence of a maximum SPR at a wavelength of 280 nm (Figure 1A) revealed the absorption of light by the MgO-NPs at that specific wavelength. SPR occurs when the free electrons on the surface of NPs are excited by incident light. The observation of SPR is a critical factor confirming the successful formation and stability of MgO-NPs. The absorption peak at 280 nm suggests that the NPs in this study possessed unique optical properties related to their size, shape, and composition. The obtained results were in agreement with published data from the literature, which reported that the maximum SPR of MgO-NPs was in the range of 260–280 nm [28,29]. Also, the highest peaks for MgO-NPs synthesized using *Tecoma stans* (L.) were observed at 281 nm [30]. Prospective MgO-NP sizes are related to SPR, with smaller sizes being observed when SPR is positioned at shorter wavelengths (<300 nm) and larger sizes being found when SPR is located at longer wavelengths (>300 nm) [31].

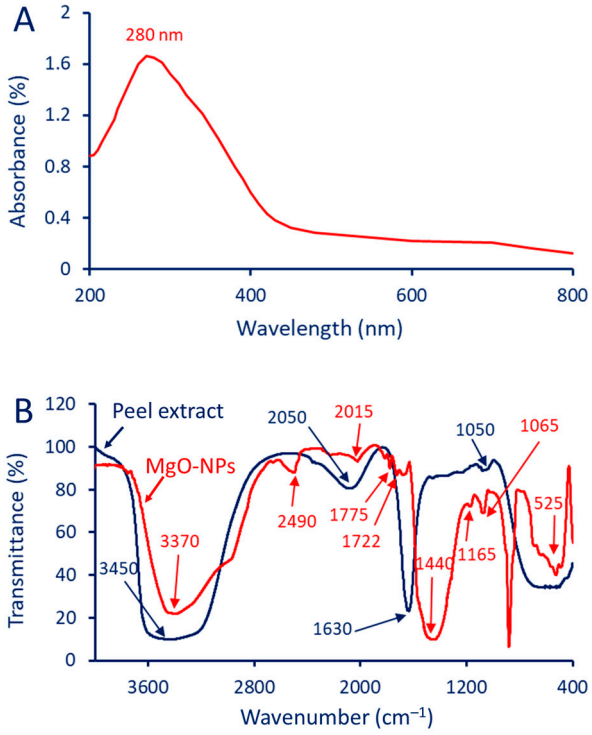

Figure 1. UV-Vis spectroscopy (**A**) and FT-IR chart (**B**) of green synthesized MgO-NPs.

3.1.2. FT-IR

Different peaks at different wavenumbers are seen in the FT-IR spectra of both the pomegranate peel extract and synthesized MgO-NPs. As shown, the chemical changes that took place during the green synthesis of MgO-NPs can be deduced by comparing the peaks before and after the synthesis (Figure 1B). The FT-IR analysis of the peel extract contains four peaks at wavenumbers of 3450, 2050, 1630, and 1050 cm^{-1}. The intensity of these peaks was changed, and additionally, it shifted (before or after), or there appeared new peaks in the MgO-NPs. The peak at 3450 cm^{-1} corresponds to hydroxyl functional groups (–OH) in phenol, alcohol, and carboxylic acids [32]. This peak was shifted to 3370 cm^{-1} after the fabrication of the MgO-NPs. The peaks at wavenumbers 2050 and 1630 cm^{-1} correspond to the stretching vibrations of C≡N (nitrile group) and C=O (carbonyl group), respectively [33,34]. The peak 1050 cm^{-1} is associated with stretching C–O bonds for carboxylic acids, alcohol, or phenols [35]. The MgO-NP peak at 2490 cm^{-1} signifies the nitrogen-containing groups such as those with -C≡N and -NH_2 (amine groups) [36]. The C≡C stretching vibration bond, which is related to alkyne or other functional groups for compounds containing a carbon triple bond, is observed at the peak of 2015 cm^{-1}. Also, the C=O for carboxylic acids or the adsorption of CO_2 on the MgO-NPs' surfaces was related to a peak at a wavenumber of 1775 cm^{-1} [33]. The observed peaks at 1722 and 1440 cm^{-1} are related to the C=O of the ester functional group (–COO-) and the binding vibration of CH_3 (methyl group), respectively [37]. Adsorbed carbonates may be indicated by a peak at 1165 cm^{-1}, which is consistent with the stretching vibrations of carbonate groups (–CO_3) [38]. The peak at 1065 cm^{-1} is characteristic of silicate or silanol (Si-O or Si-OH) groups [39]. The presence of metal-oxygen, which corresponds to Mg-O bonds, is confirmed by the peak at 525 cm^{-1}, which is compatible with published studies [16,28,29]. The FT-IR analysis indicated that the organic components present in the plant aqueous extract, including proteins, amino acids, carbohydrates, and polysaccharides, played a role in reducing magnesium ions and providing capping and stability to the phyco-synthesized MgO-NPs.

3.1.3. Crystallinity Investigation—XRD

The crystalline nature and crystallographic structure of the MgO-NPs fabricated by the aqueous peel extract of pomegranate were analyzed by using XRD. As shown, five intense peaks, 111, 200, 221, 311, and 222, were observed at 2-theta degrees of 36.8°, 42.7°, 62.3°, 74.6°, and 78.7°, respectively (Figure 2). The peak positions at specific 2-theta degrees indicate the crystalline nature and crystallographic structure of the biosynthesized MgO-NPs according to the JCPDS file number 75-0447 [16]. Similarly, the XRD analysis of MgO-NPs fabricated by an aqueous extract of Rosa floribunda showed five intense peaks, 111, 200, 221, 311, and 222, at 2-theta degrees of 36.9°, 42.2°, 62.2°, 74.4°, and 78.5° [40]. Based on XRD analysis, the position and intensity of these peaks provide valuable information about the crystalline structure of the synthesized MgO-NPs. The presence of these sharp and intense peaks indicates that the plant-based MgO-NPs have a well-defined crystalline structure with distinct crystallographic orientations.

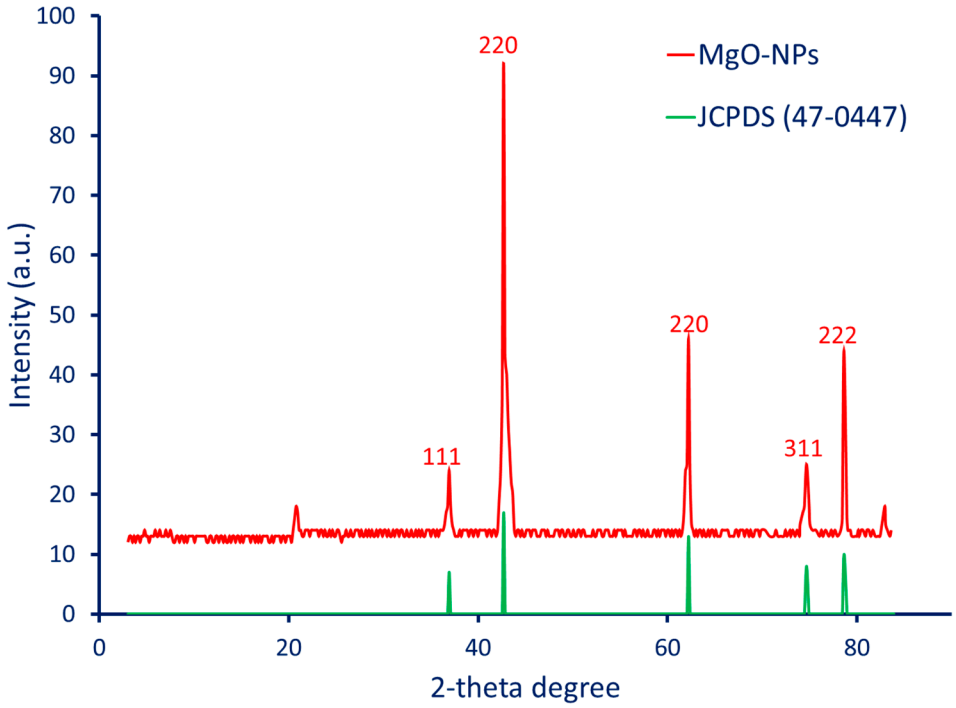

Figure 2. X-ray diffraction (XRD) analysis of *P. granatum*-mediated biosynthesis of MgO-NPs.

The crystallite size of plant-mediated MgO-NPs was calculated according to XRD analysis by using the Debye–Scherrer equation. This calculation was achieved based on the width of the highest peak (200) in XRD, located at the 2-theta value of 42.7°. Data analysis revealed that the crystallite size of the green synthesized MgO-NPs was 40 nm. In a recent study, the crystallite size of MgO-NPs synthesized by an aqueous extract of brown algae (*Cystoseira crinita*) was detected using XRD analysis to be 21 nm [41].

3.1.4. Morphological and Elemental Analysis—TEM and SEM

The size, shape, size distribution, and elemental composition of plant-synthesized MgO-NPs were investigated by TEM and EDX analysis. As shown, the aqueous extract of P. granatum has the efficacy in fabricating spherical-shaped and well-arranged NPs with sizes in the range of 10–45 nm and an average size of 24.82 ± 8.85 nm (Figure 3A,B). The determination of the size and shape of NPs is a critical factor affecting their activity. For instance, the inhibition percentages of Bacillus subtilis after being treated with MgO-NPs varies based on their sizes. In a study, the maximum inhibition percentage was 96.1% at a size of 35.9 nm and decreased to 94.5% and 75.7% at sizes of 47.3 and 2145.9 nm, respectively [42]. Also, the bacteriocidal efficacy of MgO-NPs against *B. subtilis* ATCC 9372

was at a percentage of 97.5% at size 26 nm and decreased to 93.1% at a size 69.1 nm. On the other hand, no significant difference has been noted between inhibition percentages (99.8–99.9%) of *Staphylococcus aureus* ATCC 6538 after treatment with different sizes (7.6, 14.4, 26, 35.9, 47.3, 56.3, and 69.1 nm) of MgO-NPs [43]. Therefore, due to the small size of synthesized MgO-NPs in the current study, we expect to have high biomedical activity.

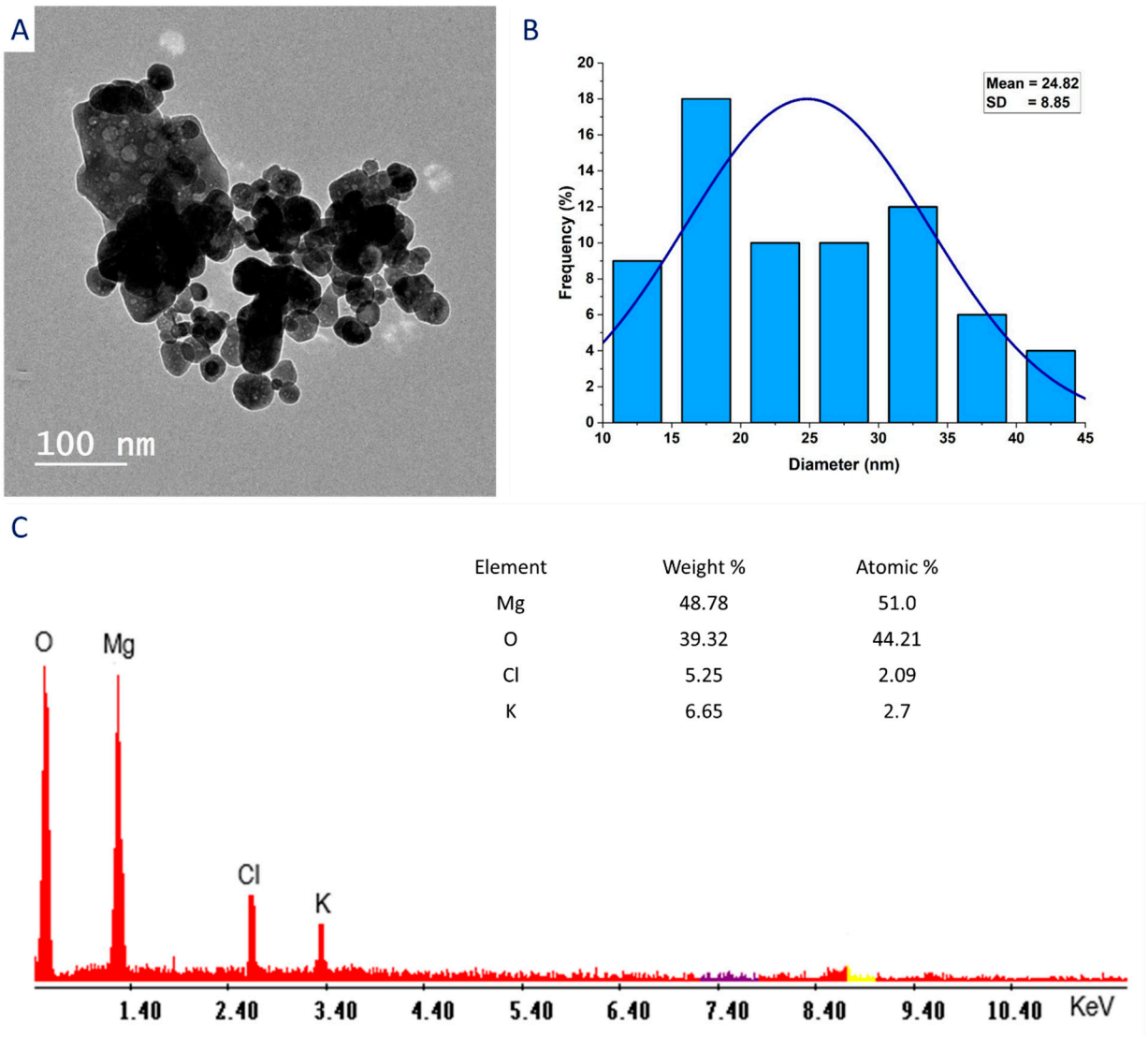

Figure 3. Characterization of green synthesized MgO-NPs including transmission electron microscopy (**A**), size distribution based on TEM imagery (**B**), and EDX analysis showing elemental composition (**C**).

The EDX analysis showed the elemental composition of biosynthesized MgO-NPs (Figure 3C). The presence of O and Mg peaks at bending energy in the range of 0.5–1.5 KeV indicates the successful formation of MgO-NPs [44]. Moreover, Figure 3C shows that the main components of MgO-NPs were Mg and O with weight and atomic percentages of 48.78 and 39.32% and 51.0 and 44.21%, respectively. Similarly, the main components of MgO-NPs fabricated by a plant extract of *Rosa floribunda* were Mg and O with weight and atomic percentages of 39.49 and 44.77% and 28.33 and 48.81%, respectively [40]. The EDX chart showed the presence peaks for Cl and K with low weight and atomic percentages. These peaks may originate from bioactive metabolites that exist in *P. granatum*-peel aqueous extract and have dual roles as reducing and stabilizing agents for MgO-NPs [45].

3.1.5. DLS Analysis

Both the size distribution of MgO-NPs in colloidal dispersion as well as their hydrodynamic residue can be detected using diffraction light scattering (DLS). As shown, the average size of green synthesized MgO-NPs in the colloidal dispersion was 58.9 nm based on the graph of size distribution. As shown, the average size of MgO-NPs varied according to different analyses. The size obtained by using DLS was larger than the size obtained by using XRD and TEM. The observed finding can be related to the differences in the conditions of analysis between TEM and DLS. TEM analysis is conducted on dry particles while DLS measurements are performed in an aqueous solution, accounting for the variation in particle diameter determination. DLS provides the hydrodynamic diameter, reflecting the size of particles in their hydrated state. Furthermore, the diameter obtained by DLS analysis may be influenced by the uneven distribution of NPs in the colloidal dispersion and the presence of coating agents from the plant extract around the NPs, introducing potential interference during size calculations [46]. Similarly, the size of MgO-NPs synthesized by using an aqueous extract of strawberry was 100 nm, according to TEM analysis, and increased to 119 nm based on DLS [47].

On the other hand, the DLS analysis gives information about the polydispersity index (PDI) of the NPs. The PDI provides important insights into the uniformity of particle sizes within the NP sample. The scale of the PDI has a range from 0 to 1. A PDI score below 0.4 indicates suspension homogeneity. On the other hand, a PDI score greater than 1 suggests that the suspension is highly heterogeneous [48]. In the current study, the PDI value of the MgO-NPs was 0.231, which indicates that the distribution of particle sizes within the synthesized NPs was relatively narrow and more uniform. This suggests that a significant portion of the NPs in the sample had similar sizes, contributing to a well-defined size distribution. A lower PDI value often implies better control over the synthesis process, resulting in NPs with consistent sizes. Overall, the current PDI value is a promising result, indicating that the synthesis process yielded MgO-NPs with relatively uniform particle sizes, which could be advantageous for integration into various applications where consistent particle size is desired, such as in catalysis, drug delivery, or electronics [41]. In a similar study, the PDI value of phytosynthesized MgO-NPs derived from an aqueous extract of *Pterocarpus marsupium* was 0.248 [17].

3.1.6. Electrokinetic Potential

The movement of NPs in a colloidal dispersion when subjected to an electric field is represented by the zeta potential (ζ), sometimes called the electrokinetic potential. This instrument of analysis is reliable and user-friendly to investigate the electrostatic charge on the surfaces of NPs in a colloidal dispersion and provides insights into their stability and aggregation, as the changes in these features significantly affect a nanoparticle's biological function [49]. In the current study, a ζ value of -32.6 mV for plant-synthesized MgO-NPs indicated a high level of stability. The stability of NP dispersions can be characterized by their ζ values. ζ levels between ± 10 and ± 20 mV are classified as generally stable, while ζ values between ± 0 and ± 10 mV are classified as severely unstable. Moderately stable dispersions have ζ values between ± 20 and ± 30 mV, and highly stable dispersions have ζ values greater than ± 30 mV. In general, higher magnitudes of ζ (positive or negative) indicate stronger electrostatic repulsion between NPs, which helps prevent their aggregation and promotes stability. Herein, the negative ζ value for the synthesized MgO-NPs (value = -32.6 mV) indicates that these NPs had a robust net-negative charge on their surfaces. This strong negative charge increases electrostatic repulsion between particles, which reduces the particles' aggregation tendency and guarantees their stability.

3.2. Antimicrobial Activity

The emergence of multi-drug-resistant microbes (MRM) is a considerable challenge in both healthcare and agriculture. These MRM strains have advanced mechanisms to tolerate the effects of antibiotics, making their infections harder to treat and control. As

a result, scientists are actively investigating novel approaches such as the synthesis of new active compounds like NPs, which have unique properties that can improve their antimicrobial activity including their large surface area, small size, and ability to permeate microbial cells [9]. Herein, MgO-NPs were fabricated by using the green method by utilizing the metabolites in a *P. granatum* aqueous extract to act as reducing and stabilizing agents for the conversion of the metal precursor to MgO-NPs. This approach offers numerous advantages, overcoming the disadvantages of chemical and physical methods. Green synthesis is eco-friendly and sustainable, reduces the use of hazardous solvents and chemicals, is an energy-intensive method, is cost-effective, and shows biodegradability and biocompatibility [13,50]. In the current study, the potential of green synthesized MgO-NPs for countering different pathogenic microbes, including *Bacillus subtilis*, *Staphylococcus aureus*, *Pseudomonas aeruginosa*, *Escherichia coli*, and *Candida albicans*, was investigated. Data analysis showed that the antimicrobial activity of MgO-NPs occurred in a concentration-dependent manner. This phenomenon was compatible with several published studies [29,51]. As shown, the highest antimicrobial activity was observed at a high MgO-NP concentration (200 mL^{-1}) with inhibition zones of 14.3 ± 0.5, 15.7 ± 0.6, 19.7 ± 0.6, 17.3 ± 0.5, and 15.7 ± 0.6 mm for *B. subtilis*, *S. aureus*, *P. aeruginosa*, *E. coli*, and *C. albicans*, respectively (Figure 4). The diameters of these inhibition zones were decreased at low concentrations. For instance, the inhibition zones formed due to treatment with 50 mL^{-1} were 10.7 ± 0.6, 10.5 ± 0.6, 14.3 ± 0.7, 12.7 ± 0.5, and 11.3 ± 0.6 mm for the same previous sequence of microorganisms. Similarly, the inhibition zones formed due to the treatment of *P. aeruginosa*, *Aeromonas baumannii*, *Streptococcus pneumoniae*, and *E. coli* with green synthesized MgO-NPs at a concentration of 30 mL^{-1} were 8, 7, 8, and 7 mm, respectively. These inhibition zones decreased at a concentration of 10 mL^{-1} to be 6, 2, 1, and 3 mm for the same sequence of bacterial species [51]. Also, Nguyen et al. [52] reported that the adhesion properties of human pathogenic bacteria (*P. aeruginosa*, *S. aureus*, and MRSA) and yeasts (*C. albicans* and *C. glabrata*) after treatment with MgO-NPs were increased at high concentrations (1400 and 1600 μg mL^{-1}) and decreased at low concentrations.

The determination of minimum inhibitory concentration (MIC) is an important step in exploring the effectiveness of active compounds and understanding their potential for countering different pathogenic microbes. This value represents the lowest concentration of the active substance needed to inhibit or stop microbial growth. The detection of the MIC value is important to provide data regarding microbial resistance or sensitivity toward active substances. These data are significantly important in the selection of antibiotics, optimizing concentration, decreasing the emergence of antibiotic-resistant microbes, comparing the antimicrobial activities of various compounds, identifying new strategies for combating infectious diseases, helping in drug formulation and clinical decision-making, and contributing to the development of effective treatment protocols [23]. In the current study, the MIC value for the green synthesized MgO-NPs was 25 mL^{-1} for *P. aeruginosa*, *E. coli*, *B. subtilis*, and *C. albicans* with inhibition zones in the range of 8.7 to 12 mm (Figure 4). On the other hand, *S. aureus* was more resistant toward low concentrations, and hence, it had a MIC value of 50 mL^{-1} with an inhibition zone of 10.7 ± 0.7 mm.

As shown, the green synthesized MgO-NPs exhibit potent antimicrobial activity against a broad spectrum of Gram-positive bacteria and Gram-negative bacteria. Their antibacterial mechanisms involve various processes that contribute to the inhibition of bacterial growth. One of these mechanisms is their efficacy in disrupting or changing cell-membrane integrity. Some unique characteristics of green synthesized MgO-NPs, such as their small size and high surface area, enable their interaction with microbial cell membrane, leading to lipid bilayer damage, and hence increase or disrupt the selective permeability function of cell membrane [13,53]. As a result of the destruction of the cell membrane, the essential components (such as macromolecules and ions) leak out of the cells, ultimately resulting in the dysfunction of cellular homeostasis, impaired metabolism, loss of vital nutrients, and, finally, cell death [54].

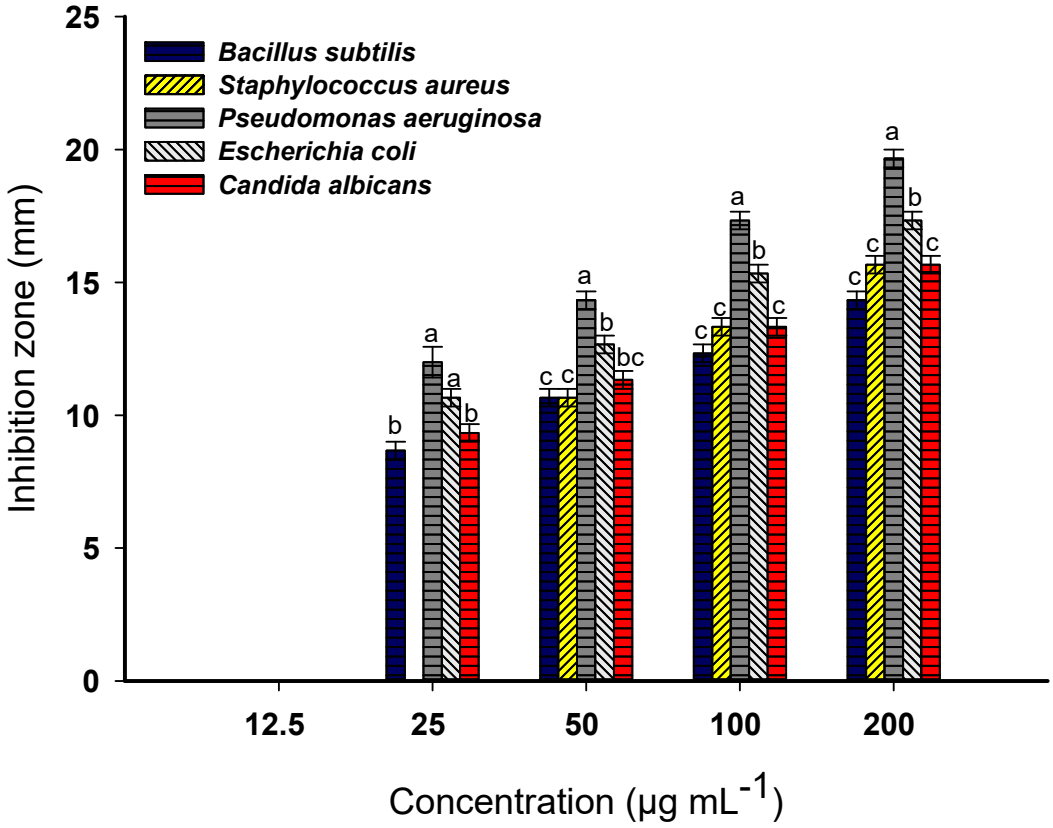

Figure 4. Antimicrobial activity of plant-based MgO-NPs against Gram-positive bacteria, Gram-negative bacteria, and unicellular fungi. The different letters at the same concentration indicate that the data are statistically significant differences ($p \leq 0.05$, $n = 3$, error bars are ±SD).

In addition to causing the disruption of the cell membrane, MgO-NPs have efficacy in producing reactive oxygen species (ROS), such as superoxide radicals (O_2^-), hydroxyl radicals ($^{\bullet}OH$), and hydrogen peroxide (H_2O_2), which have a significant role in antimicrobial activity. These free radicals induce oxidative stress, which causes cellular component damage (such as that of DNA, lipids, proteins, and amino acids), leading to microbial cell death [55,56]. Moreover, microbial cell wall structure plays a significant role in explaining the antimicrobial activity of MgO-NPs. Gram-positive bacteria have a thick peptidoglycan layer, compared to Gram-negative bacteria, which acts as a barrier to prevent the penetration of MgO-NPs [27]. This explains the high antibacterial activity of MgO-NPs toward Gram-negative bacteria compared to Gram-positive bacteria. Another inhibitory mechanism of MgO-NPs is a discharge of toxic ions (Mg^{2+}) upon entry into cells. These toxic ions can interact with amino acids (thiol group), leading to the destruction of the normal structures of proteins and, hence, cell death [51]. There is a further inhibitory mechanism of MgO-NPs which works through their potential to inhibit vital enzymatic processes in microbes. They can disrupt metabolic processes and slow or inhibit cell growth by, for instance, blocking enzymes necessary for energy production and cellular respiration [57].

Regarding *C. albicans*, the activity of MgO-NPs is slightly different. MgO-NPs can directly interact with the fungal cell wall, leading to structural changes in cell wall components (chitin and sterol pattern) and destabilization. This disruption weakens the integrity of the fungal cell wall and compromises its protective function. Furthermore, MgO-NPs can enhance oxidative stress in *C. albicans* cells via the production of ROS. The oxidative stress disrupts key cellular processes and causes damage to DNA, lipids, and proteins, ultimately leading to cell death [58]. The combined action of cell wall disruption and oxidative stress contributes to the potent antifungal activity of MgO-NPs against *C. albicans*.

3.3. Mosquitocidal Activity

Recently, the consideration of sustainable and effective solutions to combat mosquito-borne diseases has driven important attention toward the discovery of new active compounds with mosquitocidal properties. Among the different approaches explored, the use of NPs has emerged as a promising tool for this purpose [59]. The unique properties of these nanoscale materials offer an exciting prospect for the control of mosquitoes. One particular nanoparticle that has garnered significant interest is the MgO-NP. Data analysis has shown that the mortality percentages of *Culex quinquefasciatus* due to MgO-NPs treatment are dependent on NP concentrations and incubation times. This observation has been matched with published investigations. For instance, the activity of plant-mediated Cadmium Sulphide (CdS) NPs on the mortality percentages of *C. pipiens* was found to be concentration-dependent [60]. Also, the mortality percentages of *C. quinquefasciatus* and *Aedes aegypti* due to treatment with silver NPs fabricated using isoamyl acetate obtained from a leaf aqueous extract were concentration-dependent [8]. In the current study, the mortality percentages with 10 μg mL^{-1} were 0.0 ± 0.0, 17.4 ± 3.4, and 30.7 ± 5.8% after 24, 48, and 72 h, respectively (Table 1). These percentages were increased to be 14.1 ± 3.7, 31.9 ± 2.1, and 53.8 ± 1.8% and 29.6 ± 3.1, 43.9 ± 3.9, and 88.3 ± 3.2%, after treatment with 50 and 100 μg mL^{-1}, respectively, for 24, 48, and 72 h.

Table 1. Mosquitocidal activity (Larvicidal mortality, pupa mortality, and adult emergence) of biosynthesized MgO-NPs at different concentrations against 3rd-instar larvae of *C. quinquefasciatus* for different interval times (24, 48, and 72 h).

Conc. (μg mL^{-1})	Larval Mortality (%) 3rd Larval Instar			Malformed Pupae (%)	Pupal Mortality (%)	Adult Emergence (%)
	24 h	48 h	72 h			
Control	0.0 ± 0.0	0.0 ± 0.0	0.0 ± 0.0	0.0	0.0	100
100	29.6 ± 3.1	43.9 ± 3.9	88.3 ± 3.2	11.7	100	0.0
75	20.8 ± 1.9	37.5 ± 2.7	67.2 ± 3.7	32.8	100	0.0
50	14.1 ± 3.7	31.9 ± 2.1	53.8± 1.8	46.2	100	0.0
25	9.4 ± 2.1	20.3 ± 4.0	39.2 ± 4.2	60.8	100	0.0
10	0.0 ± 0.0	17.4 ± 3.7	30.7 ± 5.8	69.3	100	0.0

In a similar study, various metal oxide NPs including silicon dioxide NPs (SiO_2-NPs), MgO-NPs, zinc oxide NPs (ZnO-NPs), and copper oxide NPs (CuO-NPs) showed mortality in 3rd-instar *C. quinquefasciatus* with percentages of 46.0 ± 8.2, 43.1 ± 9.4, 33.2 ± 12.5, and 66.3 ± 4.7%, respectively after 48 h at a concentration of 500 μg mL^{-1} [61]. The mosquitocidal activity of MgO-NPs varied based on the synthesized methods. For example, the mortality percentages of *Aedes albopictus* and *A. aegypti* after treatment with green synthesized MgO-NPs with a concentration of 50 μg mL^{-1} were 76 and 74%, respectively compared to the mortality percentages for those synthesized by hydrothermal, sol-gel, and microwave method (88 and 92%, 82 and 84%, and 74 and 76%, respectively) at the same concentration [18]. Interestingly, all pupae that originated from the last bioassay time (72 h) were malformed and hence did not hatch to adults (all pupa mortality percentages were 100%; all adult emergency percentages were 0.0%) (Table 1). Incompatible with the obtained results, the treatment of the 3rd instar of *C. pipiens* by CdS-NPs caused mortality percentages for larvae and pupae with values of 51 ± 1.01 and 18.4 ± 0.2%, respectively, and the percentage of malformed pupae was 8.2 ± 0.3% [60].

As shown, the plant-mediated-MgO-NPs have shown promising mosquitocidal activity toward 3rd-instar larvae, pupae, and, hence, the percentages of hatched adults of *C. quinquefasciatus*. This hopeful activity could be attributed to the efficacy of MgO-NPs in damaging a mosquito's cuticle, which is considered the first protective outer layer. The damage of the cuticle layer causes osmotic stress, the loss of hair/setae, depigmentation, the dissolving of wax layers, the loss of distinction between exo- and endocuticle, dehydration, and, ultimately, insect death [62]. Moreover, MgO-NPs can enhance the production of

ROS such as OH^- and O_2^- radicals, which induce oxidative stress inside the mosquito's body, leading to DNA, lipid, and protein damage, and, hence, cell death [18]. In order to breathe, mosquitoes need a complex system of air tubes (called tracheae) that allow for gas exchange. When breathed in or swallowed, MgO-NPs can block these tracheae, causing respiratory failure and death [2]. Mosquito larvae rely heavily on digestive enzymes to break down the organic substances they consume in water. MgO-NPs have efficacy in inhibiting these enzymes' functioning; they can impede the larvae's ability to digest food and absorb nutrients, stunting their development [63]. On the other hand, MgO-NPs can interact with the nervous systems of mosquitoes by passing the blood–brain barrier and interfering with neurotransmission, leading to neural toxicity and neurological dysfunction, which can result in paralysis or death in mosquitoes [62]. Finally, some larvae depend on specific microorganisms such as bacteria and microalgae in their diet. Due to the antimicrobial properties of MgO-NPs, MgO-NPs can inhibit the growth of these microorganisms and hence disrupt the food chain for these larvae, having a negative impact on their development and survival [64]. It is important to note that MgO-NPs can have a wide range of mosquitocidal mechanisms depending on some important aspects including particle size, concentration, exposure time, and the mosquito species being combated.

4. Conclusions

In summary, MgO-NPs were successfully synthesized using a *P. granatum*-peel aqueous extract, offering a green, safe, eco-friendly, and cost-effective approach. Characterization through UV-Vis spectroscopy, FT-IR, TEM, XRD, DLS, and zeta potential revealed their properties: they were spherical, well arranged, and crystalline in nature, with sizes of 10–45 nm. These plant-based MgO-NPs displayed potent antimicrobial activity against various bacteria (*B. subtilis*, *S. aureus*, *E. coli*, and *P. aeruginosa*) and fungi (*C. albicans*) with low MIC values (25–50 µg mL^{-1}). Additionally, they exhibited remarkable larvicidal effects on *C. quinquefasciatus*, resulting in high mortality rates (88.3%) and malformed pupae, preventing adult emergence (100%). Overall, these MgO-NPs hold significant potential for inhibiting pathogenic microorganisms and controlling larvae and pupae at low concentrations.

Author Contributions: Conceptualization, A.F., K.S.A. and A.M.E.; methodology, A.F., A.M.E., A.M.A., M.A.A. and M.F.H.; software, A.F., K.S.A., A.M.A. and M.I.A.; validation, A.F., K.S.A., M.I.A. and A.M.E.; formal analysis, A.F., M.A.A., A.M.A. and M.F.H.; investigation, M.A.A. and M.F.H.; resources, A.F., K.S.A., M.I.A. and M.A.A.; data curation, A.F. and A.M.A.; writing—original draft preparation, A.F., K.S.A., A.M.E. and M.A.A.; writing—review and editing, A.F., A.M.E. and M.F.H.; visualization, A.F., K.S.A., M.I.A. and A.M.A.; supervision, A.F. and K.S.A.; project administration, A.F., A.M.E., A.M.A., M.A.A. and M.F.H.; funding acquisition, A.F., K.S.A. and M.F.H. All authors have read and agreed to the published version of the manuscript.

Funding: This work was supported and funded by the Deanship of Scientific Research at Imam Mohammad Ibn Saud Islamic University (IMSIU) (grant number IMSIU-RP23027).

Data Availability Statement: The data presented in this study are available on request from the corresponding authors.

Acknowledgments: The authors extend their appreciation to the Botany and Microbiology Department, Faculty of Science, Al-Azhar University, Cairo, Egypt for the great support in the achievement and publication of this research work. Furthermore, the authors acknowledge the support from Imam Mohammad Ibn Saud Islamic University Riyadh, Saudi Arabia.

Conflicts of Interest: The authors declare no conflict of interest.

References

1. Jamrozik, E.; Selgelid, M.J. Drug-Resistant Infection: Causes, Consequences, and Responses. In *Ethics and Drug Resistance: Collective Responsibility for Global Public Health*; Jamrozik, E., Selgelid, M., Eds.; Springer International Publishing: Cham, Switzerland, 2020; pp. 3–18.
2. Nie, D.; Li, J.; Xie, Q.; Ai, L.; Zhu, C.; Wu, Y.; Gui, Q.; Zhang, L.; Tan, W. Nanoparticles: A Potential and Effective Method to Control Insect-Borne Diseases. *Bioinorg. Chem. Appl.* **2023**, *2023*, 5898160. [CrossRef] [PubMed]
3. Karnwal, A.; Kumar, G.; Pant, G.; Hossain, K.; Ahmad, A.; Alshammari, M.B. Perspectives on Usage of Functional Nanomaterials in Antimicrobial Therapy for Antibiotic-Resistant Bacterial Infections. *ACS Omega* **2023**, *8*, 13492–13508. [CrossRef] [PubMed]
4. Mohamed, A.E.; Elgammal, W.E.; Eid, A.M.; Dawaba, A.M.; Ibrahim, A.G.; Fouda, A.; Hassan, S.M. Synthesis and characterization of new functionalized chitosan and its antimicrobial and in-vitro release behavior from topical gel. *Int. J. Biol. Macromol.* **2022**, *207*, 242–253. [CrossRef] [PubMed]
5. Nassar, A.A.; Atta, H.M.; Abdel-Rahman, M.A.; El Naghy, W.S.; Fouda, A. Myco-synthesized copper oxide nanoparticles using harnessing metabolites of endophytic fungal strain *Aspergillus terreus*: An insight into antibacterial, anti-Candida, biocompatibility, anticancer, and antioxidant activities. *BMC Complement. Med. Ther.* **2023**, *23*, 261. [CrossRef] [PubMed]
6. Choi, L.; Pryce, J.; Richardson, M.; Lutje, V.; Walshe, D.; Garner, P. *Guidelines for Malaria Vector Control*; World Health Organization: Geneva, Switzerland, 2019; pp. 1–171.
7. Reis, L.A.; Silva, E.V.; Dias, D.D.; Freitas, M.N.; Caldeira, R.D.; Araújo, P.A.; Silva, F.S.; Rosa Junior, J.W.; Brandão, R.C.; Nascimento, B.L.; et al. Vector Competence of *Culex quinquefasciatus* from Brazil for West Nile Virus. *Trop. Med. Infect. Dis.* **2023**, *8*, 217. [CrossRef]
8. Velayutham, K.; Ramanibai, R. Larvicidal activity of synthesized silver nanoparticles using isoamyl acetate identified in *Annona squamosa* leaves against *Aedes aegypti* and *Culex quinquefasciatus*. *J. Basic Appl. Zool.* **2016**, *74*, 16–22. [CrossRef]
9. Khezerlou, A.; Alizadeh-Sani, M.; Azizi-Lalabadi, M.; Ehsani, A. Nanoparticles and their antimicrobial properties against pathogens including bacteria, fungi, parasites and viruses. *Microb. Pathog.* **2018**, *123*, 505–526. [CrossRef]
10. Vijayaram, S.; Razafindralambo, H.; Sun, Y.Z.; Vasantharaj, S.; Ghafarifarsani, H.; Hoseinifar, S.H.; Raeeszadeh, M. Applications of Green Synthesized Metal Nanoparticles—A Review. *Biol. Trace Elem. Res.* **2023**, 1–27. [CrossRef]
11. Kulkarni, D.; Sherkar, R.; Shirsathe, C.; Sonwane, R.; Varpe, N.; Shelke, S.; More, M.P.; Pardeshi, S.R.; Dhaneshwar, G.; Junnuthula, V.; et al. Biofabrication of nanoparticles: Sources, synthesis, and biomedical applications. *Front. Bioeng. Biotechnol.* **2023**, *11*, 1159193. [CrossRef]
12. Ismael, A.F.; Ahmed, N.M.; Ibrahim, K.H.; Al-Kubaisi, A.A. Tea Plant Leaves for Green Synthesis of Metallic Nanoparticles. *Macromol. Symp.* **2023**, *407*, 2100377. [CrossRef]
13. Alsaiari, N.S.; Alzahrani, F.M.; Amari, A.; Osman, H.; Harharah, H.N.; Elboughdiri, N.; Tahoon, M.A. Plant and Microbial Approaches as Green Methods for the Synthesis of Nanomaterials: Synthesis, Applications, and Future Perspectives. *Molecules* **2023**, *28*, 463. [CrossRef] [PubMed]
14. Ramezani Farani, M.; Farsadrooh, M.; Zare, I.; Gholami, A.; Akhavan, O. Green Synthesis of Magnesium Oxide Nanoparticles and Nanocomposites for Photocatalytic Antimicrobial, Antibiofilm and Antifungal Applications. *Catalysts* **2023**, *13*, 642. [CrossRef]
15. Abdel-Maksoud, G.; Abdel-Nasser, M.; Hassan, S.E.-D.; Eid, A.M.; Abdel-Nasser, A.; Fouda, A. Green synthesis of magnesium oxide nanoparticles using probiotic strain Lactobacillus gasseri and their activity against fungal strains isolated from historical manuscripts. *Egypt. J. Chem.* **2023**, *66*, 179–189. [CrossRef]
16. Essien, E.R.; Atasie, V.N.; Okeafor, A.O.; Nwude, D.O. Biogenic synthesis of magnesium oxide nanoparticles using *Manihot esculenta* (Crantz) leaf extract. *Int. Nano Lett.* **2020**, *10*, 43–48. [CrossRef]
17. Ammulu, M.A.; Vinay Viswanath, K.; Giduturi, A.K.; Vemuri, P.K.; Mangamuri, U.; Poda, S. Phytoassisted synthesis of magnesium oxide nanoparticles from *Pterocarpus marsupium* rox.b heartwood extract and its biomedical applications. *J. Genet. Eng. Biotechnol.* **2021**, *19*, 21. [CrossRef]
18. Abinaya, S.; Kavitha, H. Magnesium Oxide Nanoparticles: Effective Antilarvicidal and Antibacterial Agents. *ACS Omega* **2023**, *8*, 5225. [CrossRef]
19. Bawazeer, S.; Rauf, A.; Nawaz, T.; Khalil, A.A.; Javed, M.S.; Muhammad, N.; Shah, M.A. *Punica granatum* peel extracts mediated the green synthesis of gold nanoparticles and their detailed in vivo biological activities. *Green Process. Synth.* **2021**, *10*, 882–892. [CrossRef]
20. Santos, É.S.; Hoscheid, J.; da Mata, P.T.G. Antibacterial activity of crude ethanolic and fractionated extracts of *Punica granatum* Linn. fruit peels. *Rev. Ciências Farm. Básica Apl.* **2015**, *36*, 219–225.
21. Bokuniaeva, A.O.; Vorokh, A.S. Estimation of particle size using the Debye equation and the Scherrer formula for polyphasic TiO_2 powder. *J. Phys. Conf. Ser.* **2019**, *1410*, 012057. [CrossRef]
22. Balouiri, M.; Sadiki, M.; Ibnsouda, S.K. Methods for in vitro evaluating antimicrobial activity: A review. *J. Pharm. Anal.* **2016**, *6*, 71–79. [CrossRef]
23. Kowalska-Krochmal, B.; Dudek-Wicher, R. The Minimum Inhibitory Concentration of Antibiotics: Methods, Interpretation, Clinical Relevance. *Pathogens* **2021**, *10*, 165. [CrossRef] [PubMed]
24. Kauffman, E.; Payne, A.; Franke, M.A.; Schmid, M.A.; Harris, E.; Kramer, L.D. Rearing of *Culex* spp. and *Aedes* spp. Mosquitoes. *Bio-Protoc.* **2017**, *7*, e2542. [CrossRef] [PubMed]

25. Fouda, A.; Awad, M.A.; Eid, A.M.; Saied, E.; Barghoth, M.G.; Hamza, M.F.; Awad, M.F.; Abdelbary, S.; Hassan, S.E. An Eco-Friendly Approach to the Control of Pathogenic Microbes and *Anopheles stephensi* Malarial Vector Using Magnesium Oxide Nanoparticles (Mg-NPs) Fabricated by *Penicillium chrysogenum*. *Int. J. Mol. Sci.* **2021**, *22*, 5096. [CrossRef] [PubMed]
26. El-khamissi, H.; El-Hamamsy, S. Phytochemicals, Antioxidant Activity and Identification of Phenolic Compounds by HPLC of Pomegranate (*Punica granatum* L.) Peel Extracts. *J. Agric. Chem. Biotechnol.* **2020**, *11*, 5837. [CrossRef]
27. Hassan, S.E.; Fouda, A.; Saied, E.; Farag, M.M.S.; Eid, A.M.; Barghoth, M.G.; Awad, M.A.; Hamza, M.F.; Awad, M.F. Rhizopus oryzae-Mediated Green Synthesis of Magnesium Oxide Nanoparticles (MgO-NPs): A Promising Tool for Antimicrobial, Mosquitocidal Action, and Tanning Effluent Treatment. *J. Fungi* **2021**, *7*, 372. [CrossRef]
28. Moorthy, S.K.; Ashok, C.H.; Rao, K.V.; Viswanathan, C. Synthesis and Characterization of Mgo Nanoparticles by Neem Leaves through Green Method. *Mater. Today Proc.* **2015**, *2*, 4360–4368. [CrossRef]
29. Vergheese, M.; Vishal, S.K. Green synthesis of magnesium oxide nanoparticles using Trigonella foenum-graecum leaf extract and its antibacterial activity. *J. Pharmacogn. Phytochem.* **2018**, *7*, 1193–1200.
30. Nguyen, D.T.C.; Dang, H.H.; Vo, D.N.; Bach, L.G.; Nguyen, T.D.; Tran, T.V. Biogenic synthesis of MgO nanoparticles from different extracts (flower, bark, leaf) of *Tecoma stans* (L.) and their utilization in selected organic dyes treatment. *J. Hazard. Mater.* **2021**, *404*, 124146. [CrossRef]
31. Jeevanandam, J.; Chan, Y.S.; Danquah, M.K. Biosynthesis and characterization of MgO nanoparticles from plant extracts via induced molecular nucleation. *New J. Chem.* **2017**, *41*, 2800–2814. [CrossRef]
32. Hamza, M.F.; Wei, Y.; Althumayri, K.; Fouda, A.; Hamad, N.A. Synthesis and Characterization of Functionalized Chitosan Nanoparticles with Pyrimidine Derivative for Enhancing Ion Sorption and Application for Removal of Contaminants. *Materials* **2022**, *15*, 4676. [CrossRef]
33. Coates, J. Interpretation of Infrared Spectra, A Practical Approach. In *Encyclopedia of Analytical Chemistry, Applications, Theory and Instrumentation. Infrared Spectroscopy in Analysis of Polymer Crystallinity*; John Wiley & Sons: Hoboken, NJ, USA, 2006.
34. Hamza, M.F.; Lu, S.; Salih, K.A.M.; Mira, H.; Dhmees, A.S.; Fujita, T.; Wei, Y.; Vincent, T.; Guibal, E. As(V) sorption from aqueous solutions using quaternized algal/polyethyleneimine composite beads. *Sci. Total Environ.* **2020**, *719*, 137396. [CrossRef]
35. El-Naggar, N.E.-A.; Hussein, M.H.; Shaaban-Dessuuki, S.A.; Dalal, S.R. Production, extraction and characterization of Chlorella vulgaris soluble polysaccharides and their applications in AgNPs biosynthesis and biostimulation of plant growth. *Sci. Rep.* **2020**, *10*, 3011. [CrossRef] [PubMed]
36. Zahra, M.H.; Hamza, M.F.; El-Habibi, G.; Abdel-Rahman, A.A.H.; Mira, H.I.; Wei, Y.; Alotaibi, S.H.; Amer, H.H.; Goda, A.E.S.; Hamad, N.A. Synthesis of a Novel Adsorbent Based on Chitosan Magnetite Nanoparticles for the High Sorption of Cr (VI) Ions: A Study of Photocatalysis and Recovery on Tannery Effluents. *Catalysts* **2022**, *12*, 678. [CrossRef]
37. Alaizeri, Z.M.; Alhadlaq, H.A.; Aldawood, S.; Akhtar, M.J.; Amer, M.S.; Ahamed, M. Facile Synthesis, Characterization, Photocatalytic Activity, and Cytotoxicity of Ag-Doped MgO Nanoparticles. *Nanomaterials* **2021**, *11*, 2915. [CrossRef]
38. Prescott, H.A.; Li, Z.-J.; Kemnitz, E.; Trunschke, A.; Deutsch, J.; Lieske, H.; Auroux, A. Application of calcined Mg–Al hydrotalcites for Michael additions: An investigation of catalytic activity and acid–base properties. *J. Catal.* **2005**, *234*, 119–130. [CrossRef]
39. Shafqat, S.S.; Khan, A.A.; Zafar, M.N.; Alhaji, M.H.; Sanaullah, K.; Shafqat, S.R.; Murtaza, S.; Pang, S.C. Development of amino-functionalized silica nanoparticles for efficient and rapid removal of COD from pre-treated palm oil effluent. *J. Mater. Res. Technol.* **2019**, *8*, 385–395. [CrossRef]
40. Younis, I.Y.; El-Hawary, S.S.; Eldahshan, O.A.; Abdel-Aziz, M.M.; Ali, Z.Y. Green synthesis of magnesium nanoparticles mediated from *Rosa floribunda* charisma extract and its antioxidant, antiaging and antibiofilm activities. *Sci. Rep.* **2021**, *11*, 16868. [CrossRef]
41. Fouda, A.; Eid, A.M.; Abdel-Rahman, M.A.; El-Belely, E.F.; Awad, M.A.; Hassan, S.E.; Al-Faifi, Z.E.; Hamza, M.F. Enhanced Antimicrobial, Cytotoxicity, Larvicidal, and Repellence Activities of Brown Algae, *Cystoseira crinita*-Mediated Green Synthesis of Magnesium Oxide Nanoparticles. *Front. Bioeng. Biotechnol.* **2022**, *10*, 849921. [CrossRef]
42. Huang, L.; Li, D.; Lin, Y.; Evans, D.G.; Duan, X. Influence of nano-MgO particle size on bactericidal action against *Bacillus subtilis* var. niger. *Chin. Sci. Bull.* **2005**, *50*, 514–519. [CrossRef]
43. Huang, L.; Li, D.-Q.; Lin, Y.-J.; Wei, M.; Evans, D.G.; Duan, X. Controllable preparation of Nano-MgO and investigation of its bactericidal properties. *J. Inorg. Biochem.* **2005**, *99*, 986–993. [CrossRef]
44. Ogunyemi, S.O.; Zhang, F.; Abdallah, Y.; Zhang, M.; Wang, Y.; Sun, G.; Qiu, W.; Li, B. Biosynthesis and characterization of magnesium oxide and manganese dioxide nanoparticles using *Matricaria chamomilla* L. extract and its inhibitory effect on Acidovorax oryzae strain RS-2. *Artif. Cells Nanomed. Biotechnol.* **2019**, *47*, 2230–2239. [CrossRef] [PubMed]
45. Abdel-Aziz, M.M.; Emam, T.M.; Elsherbiny, E.A. Bioactivity of magnesium oxide nanoparticles synthesized from cell filtrate of endobacterium *Burkholderia rinojensis* against *Fusarium oxysporum*. *Mater. Sci. Engineering. C Mater. Biol. Appl.* **2020**, *109*, 110617. [CrossRef] [PubMed]
46. Tomaszewska, E.; Soliwoda, K.; Kadziola, K.; Tkacz-Szczesna, B.; Celichowski, G.; Cichomski, M.; Szmaja, W.; Grobelny, J. Detection Limits of DLS and UV-Vis Spectroscopy in Characterization of Polydisperse Nanoparticles Colloids. *J. Nanomater.* **2013**, *2013*, 313081. [CrossRef]
47. Khan, A.U.; Khan, M.; Khan, A.A.; Parveen, A.; Ansari, S.; Alam, M. Effect of Phyto-Assisted Synthesis of Magnesium Oxide Nanoparticles (MgO-NPs) on Bacteria and the Root-Knot Nematode. *Bioinorg. Chem. Appl.* **2022**, *2022*, 3973841. [CrossRef] [PubMed]

48. Danaei, M.; Dehghankhold, M.; Ataei, S.; Hasanzadeh Davarani, F.; Javanmard, R.; Dokhani, A.; Khorasani, S.; Mozafari, M.R. Impact of Particle Size and Polydispersity Index on the Clinical Applications of Lipidic Nanocarrier Systems. *Pharmaceutics* **2018**, *10*, 57. [CrossRef] [PubMed]
49. Sizochenko, N.; Mikolajczyk, A.; Syzochenko, M.; Puzyn, T.; Leszczynski, J. Zeta potentials (ζ) of metal oxide nanoparticles: A meta-analysis of experimental data and a predictive neural networks modeling. *NanoImpact* **2021**, *22*, 100317. [CrossRef] [PubMed]
50. Fouda, A.; Saied, E.; Eid, A.M.; Kouadri, F.; Alemam, A.M.; Hamza, M.F.; Alharbi, M.; Elkelish, A.; Hassan, S.E. Green Synthesis of Zinc Oxide Nanoparticles Using an Aqueous Extract of *Punica granatum* for Antimicrobial and Catalytic Activity. *J. Funct. Biomater.* **2023**, *14*, 205. [CrossRef]
51. Pugazhendhi, A.; Prabhu, R.; Muruganantham, K.; Shanmuganathan, R.; Natarajan, S. Anticancer, antimicrobial and photocatalytic activities of green synthesized magnesium oxide nanoparticles (MgONPs) using aqueous extract of *Sargassum wightii*. *J. Photochem. Photobiology. B Biol.* **2019**, *190*, 86–97. [CrossRef]
52. Nguyen, N.-Y.T.; Grelling, N.; Wetteland, C.L.; Rosario, R.; Liu, H. Antimicrobial Activities and Mechanisms of Magnesium Oxide Nanoparticles (nMgO) against Pathogenic Bacteria, Yeasts, and Biofilms. *Sci. Rep.* **2018**, *8*, 16260. [CrossRef]
53. Nassar, A.-R.A.; Eid, A.M.; Atta, H.M.; El Naghy, W.S.; Fouda, A. Exploring the antimicrobial, antioxidant, anticancer, biocompatibility, and larvicidal activities of selenium nanoparticles fabricated by endophytic fungal strain *Penicillium verhagenii*. *Sci. Rep.* **2023**, *13*, 9054. [CrossRef]
54. Ammendolia, D.A.; Bement, W.M.; Brumell, J.H. Plasma membrane integrity: Implications for health and disease. *BMC Biol.* **2021**, *19*, 71. [CrossRef] [PubMed]
55. Slavin, Y.N.; Asnis, J.; Häfeli, U.O.; Bach, H. Metal nanoparticles: Understanding the mechanisms behind antibacterial activity. *J. Nanobiotechnology* **2017**, *15*, 65. [CrossRef] [PubMed]
56. Fouda, A.; Hassan, S.E.; Eid, A.M.; Abdel-Rahman, M.A.; Hamza, M.F. Light enhanced the antimicrobial, anticancer, and catalytic activities of selenium nanoparticles fabricated by endophytic fungal strain, *Penicillium crustosum* EP-1. *Sci. Rep.* **2022**, *12*, 11834. [CrossRef] [PubMed]
57. Stanić, V.; Tanasković, S.B. Chapter 11—Antibacterial activity of metal oxide nanoparticles. In *Nanotoxicity*; Rajendran, S., Mukherjee, A., Nguyen, T.A., Godugu, C., Shukla, R.K., Eds.; Elsevier: Amsterdam, The Netherlands, 2020; pp. 241–274.
58. Venkatappa, M.M.; Udagani, C.; Hanumegowda, S.M.; Pramod, S.N.; Venkataramaiah, S.; Rangappa, R.; Achur, R.; Alataway, A.; Dewidar, A.Z.; Al-Yafrsi, M.; et al. Effect of Biofunctional Green Synthesized MgO-Nanoparticles on Oxidative-Stress-Induced Tissue Damage and Thrombosis. *Molecules* **2022**, *27*, 5162. [CrossRef]
59. Onen, H.; Luzala, M.M.; Kigozi, S.; Sikumbili, R.M.; Muanga, C.-J.K.; Zola, E.N.; Wendji, S.N.; Buya, A.B.; Balciunaitiene, A.; Viškelis, J.; et al. Mosquito-Borne Diseases and Their Control Strategies: An Overview Focused on Green Synthesized Plant-Based Metallic Nanoparticles. *Insects* **2023**, *14*, 221. [CrossRef] [PubMed]
60. Aly, M.; Osman, K.; Omar, E.; Mahmoud, M. Recent, Eco-friendly Approach for Controlling *Culex pipiens* (L.) using Novel Synthesized Cadmium Sulphide Nanoparticles of *Ocimum basillicum* Extract. *Egypt. J. Aquat. Biol. Fish.* **2021**, *25*, 359–377.
61. Chakrabarti, A.; Patra, P. Relative larvicidal property of common oxide nanostructures against *Culex quinquefasciatus*. *IET Nanobiotechnol.* **2020**, *14*, 389–395. [CrossRef]
62. Shahzad, K.; Manzoor, F. Nanoformulations and their mode of action in insects: A review of biological interactions. *Drug Chem. Toxicol.* **2021**, *44*, 1–11. [CrossRef]
63. Misyura, L.; Grieco Guardian, E.; Durant, A.C.; Donini, A. A comparison of aquaporin expression in mosquito larvae (*Aedes aegypti*) that develop in hypo-osmotic freshwater and iso-osmotic brackish water. *PLoS ONE* **2020**, *15*, e0234892. [CrossRef]
64. Souza, R.S.; Virginio, F.; Riback, T.I.S.; Suesdek, L.; Barufi, J.B.; Genta, F.A. Microorganism-Based Larval Diets Affect Mosquito Development, Size and Nutritional Reserves in the Yellow Fever Mosquito *Aedes aegypti* (Diptera: Culicidae). *Front. Physiol.* **2019**, *10*, 152. [CrossRef]